

Efficiency of Thin Magnetically-Arrested Disks Around Black Holes

Mark J. Avara^{1*}, Jonathan C. McKinney^{2,3}, Christopher S. Reynolds^{1,2}

¹ *University of Maryland at College Park, Dept. of Astronomy, 1113 Physical Sciences Complex, College Park, MD 20742, USA*

² *Joint Space-Science Institute, 1113 Physical Sciences Complex, College Park, MD 20742, USA*

³ *University of Maryland at College Park, Dept. of Physics, 3114 Physical Sciences Complex, College Park, MD 20742, USA*

Submitted 2015 August xx. xxxxxxxxxxxx

ABSTRACT

The radiative and jet efficiencies of thin magnetized accretion disks around black holes (BHs) are affected by BH spin and the presence of a magnetic field that, when strong, could lead to large deviations from Novikov-Thorne (NT) thin disk theory. To seek the maximum deviations, we perform general relativistic magnetohydrodynamic (GRMHD) simulations of radiatively efficient thin (half-height H to radius R of $H/R \approx 0.10$) disks around moderately rotating BHs with $a/M = 0.5$. First, our simulations, each evolved for more than $70,000 r_g/c$ (gravitational radius r_g and speed of light c), show that large-scale magnetic field readily accretes inward even through our thin disk and builds-up to the magnetically-arrested disk (MAD) state. Second, our simulations of thin MADs show the disk achieves a radiative efficiency of $\eta_r \approx 15\%$ (after estimating photon capture), which is about twice the NT value of $\eta_r \sim 8\%$ for $a/M = 0.5$ and gives the same luminosity as a NT disk with $a/M \approx 0.9$. Compared to prior simulations with $\lesssim 10\%$ deviations, our result of an $\approx 80\%$ deviation sets a new benchmark. Building on prior work, we are now able to complete an important scaling law which suggest that observed jet quenching in the high-soft state in BH X-ray binaries is consistent with an ever-present MAD state with a weak yet sustained jet.

Key words: accretion, accretion discs, black hole physics, hydrodynamics, (magnetohydrodynamics) MHD, methods: numerical, gravitation

1 INTRODUCTION

Black hole (BH) accretion systems can operate as efficient engines converting gravitational potential energy and BH spin energy into radiation. Quasars, active galactic nuclei (AGN), X-ray binaries, gamma-ray bursts, and other BH accretion systems enter a thin radiatively efficient mode when the luminosity is between $\sim 10^{-2}$ and ~ 0.5 times the Eddington luminosity (Abramowicz et al. 1995; Narayan & Yi 1995). The Novikov & Thorne (1973), NT, calculation for the thin disk radiative efficiency assumes emission terminates at the inner-most stable circular orbit (ISCO). However, accretion is driven by magnetic stresses via the magneto-rotational instability (MRI) (Balbus & Hawley 1991, 1998a) or magnetic braking by large scale field threading the disk (Blandford & Payne 1982) or BH (Blandford & Znajek 1977), hereafter BZ. A fundamental question in accretion theory has been whether the NT model is applicable to actual magnetized disks where magnetic flux couples to a rotating BH and increases the radiative efficiency near the ISCO (Gammie 1999; Krolik 1999). Any extra radiative efficiency could, in principle, affect BH spin estimates obtained from Soltan’s argument (e.g., see Shapiro 2005) or from continuum emission spectrum observations (McClintock et al. 2011).

An upper limit to the amount of magnetic flux a disk and BH in steady-state can support is achieved when an accretion flow reaches the so-called magnetically-arrested disk (MAD) state, when magnetic flux accretes until magnetic forces pushing out balance gas forces pushing in (Igumenshchev et al. 2003; Narayan et al. 2003; Igumenshchev 2008; Tchekhovskoy et al. 2011; McKinney et al. 2012). If jet power scales as $P_j \propto B^2 a^2$ for magnetic field B and BH spin a/M (Blandford & Znajek 1977), then the MAD state leads to the maximum jet power. The existence of such a maximum well-defined magnetic flux for a given spin is assumed when using transient jets in BH X-ray binaries to test the BZ prediction of power vs. spin (McClintock et al. 2014). Destruction of such a strong magnetic flux could lead to such transient jets without the need for BH spin (Igumenshchev 2009; Dexter et al. 2014), while BH spin measurements may be more reliable for thin MADs that could have angular momenta aligned with the BH spin axis near the BH (Polko & McKinney 2015).

General relativistic magnetohydrodynamic (GRMHD) simulations of thin disks have found different degrees of deviations from NT theory, but in these cases there are no more than 10% fractional deviations for the radiative efficiency (Shafee et al. 2008; Noble et al. 2009; Penna et al. 2010; Noble et al. 2010, 2011). Differences in results are likely due to the amount of magnetic flux that threads the BH and disk (Penna et al. 2010). Unlike other choices for initial

* E-mail: mavara@astro.umd.edu (MJA)

conditions, the amount of magnetic flux threading the BH and disk in a MAD state is independent of the initial magnetic field strength or geometry as long as there is a plentiful supply of magnetic flux (McKinney et al. 2012; Tchekhovskoy & McKinney 2012). Numerous non-MAD GRMHD simulations of relatively thick disks have been performed (De Villiers & Hawley 2003; McKinney & Gammie 2004; De Villiers et al. 2005; McKinney 2005, 2006; Komisarov & McKinney 2007; McKinney & Narayan 2007; Fragile et al. 2007; McKinney & Blandford 2009; Narayan et al. 2012). Simulations of MADs have so far involved only relatively thick disks with no cooling (Tchekhovskoy et al. 2011; McKinney et al. 2012) and thick disks with radiative transfer (McKinney et al. 2015).

We perform fully 3D GRMHD simulations of radiatively efficient thin (half-height H to radius R of $H/R \approx 0.1$) disks around rotating BHs (dimensionless spin, $a/M = 0.5$) that reach the MAD state. We expect the MAD to maximize the radiative efficiency of thin disks and lead to the maximum deviations from the NT efficiency. First, we test how easily magnetic flux advects inward by threading the disk with weak magnetic field. Second, we setup a disk that is initially nearly MAD, let it become MAD to large radius, and then measure the radiative efficiency.

We describe the physical and numerical setup in §2, present results and provide discussions in §3, and summarize in §4.

2 FULLY 3D GRMHD THIN MAD MODEL

For this study we use the HARM GRMHD code (Gammie et al. 2003) with various improvements (McKinney & Blandford 2009; McKinney et al. 2012) with two physical setups, both with spin $a/M = 0.5$. Each was run with a low resolution, medium resolution, and high resolution for convergence testing and the high resolution was used for detailed analysis. We name the simulations in this work MADxy where x=i,f signifies whether the disk starts with enough flux to be nearly MAD in the initial, i, or only MAD in the final, f, state. y=HR,MR distinguishes the grid as high or medium resolution.

2.1 Physical Model

The initial disk is Keplerian with rest-mass density that is Gaussian in angle with a half-height-to-radius ratio $H/R \approx 0.1$ and a power-law radial distribution $\rho \propto r^{-0.6}$. Since this is not an equilibrium solution near and inside the ISCO at r_{ISCO} , the density is tapered as $\rho \rightarrow \rho(1 - .95(r_{\text{ISCO}}/R)^3)$ and truncated at r_{ISCO} . The gas internal energy density e_{gas} is obtained from the vertical hydrostatic equilibrium condition of $H/R \approx \bar{h} \equiv c_s/v_{\text{rot}}$ for sound speed $c_s \approx \sqrt{\Gamma P_{\text{gas}}/\rho}$ and rotational speed v_{rot} chosen to be Keplerian with velocity $v_K = (r/r_g)/((r/r_g)^{3/2} + a/M)$. In order to seed the MRI we use a 10% random perturbation to the pressure that obeys the ideal gas law $P_{\text{gas}} = (\Gamma - 1)e_{\text{gas}}$. We choose $\Gamma = 4/3$ because the disk is expected to be radiation dominated near the BH. We set an atmosphere for the disk with $\rho = 10^{-4}(r/r_g)^{-3/2}$ and $e_{\text{gas}} = 10^{-6}(r/r_g)^{-5/2}$.

We choose an initially purely poloidal large-scale magnetic field. With other low resolution models already performed, we know ahead of time the magnetic flux reached on the BH and throughout the disk in the quasi-steady MAD state, so we then tune our initial conditions to be either nearly MAD (for MADi) or very sub-MAD (for MADf). Net magnetic flux on the BH and through the disk out to some radius is conserved and only changes by accretion or expulsion through that radius. To reach the maximal amount

of magnetic flux threading the BH and disk, we provide a large supply, and the amount of supply ends up not mattering because it is vast compared to what ends up on the BH or in the disk near the BH.

The coordinate basis ϕ -component of the vector potential is matched to the radial gas pressure profile so that the plasma parameter $\beta = P_{\text{gas}}/P_b$ (P_b as magnetic pressure), and thus the number of critical MRI wavelengths spanning a full scale-height of the disk, is a tunable constant for all radii. For MADi runs, we found it useful to transition from MAD-flux levels to a weaker sub-MAD field beyond a transition radius, $r_{0,\text{MAD}} = 30$, with a transition function $F_{\pm} = 0.5 \pm \frac{1}{\pi} \arctan((r - r_{0,\text{MAD}})/4)$. The vector potential is then calculated by radially integrating

$$A_{\phi,r} \propto (sF_- + F_+) \sin \theta^v \cdot \begin{cases} B_0^\theta & \text{if } r > r_{\text{tr}} \\ B_{\text{tr},0}^\theta r^{(-0.6/2+3/2)/\mu} & \text{if } r \leq r_{\text{tr}} \end{cases} \quad (1)$$

where B_0^θ is the field threading the disk mid-plane at time $t=0$ necessary to start with $s = 2$ and $\beta = 200/s^2 = 50$ inside $r_{0,\text{MAD}}$, and with $\beta = 200$ elsewhere. Thus, the disk within $r_{0,\text{MAD}}$ initially has $S_d \approx 0.7$, where S_d is the number of MRI wavelengths within two disk scale heights, $S_d \lesssim 0.5$ where the MRI is suppressed (Balbus & Hawley 1998b), and MADs typically have had $S_d \lesssim 0.25$ (McKinney et al. 2012). This means the MRI is marginally suppressed in MADs. The field threading the BH horizon and within the ISCO matches to the disk values at a transition radius of $r_{\text{tr}} = 12$. $\mu = 4$ ensures the initial flux residing within r_{tr} is small enough (≈ 2.5 times smaller than what ends up on the BH plus out to r_{tr}) that the BH and the region between the horizon and r_{tr} can slowly build-up to a MAD level.

To ensure a MAD can readily develop for a thin disk, our MADf model starts with sub-MAD flux at $t=0$, with $\beta = 200$ outside r_{tr} . The solution for A_ϕ is the same as the $r > r_{\text{tr}}$ branch of Eq. 1 but with $r_{0,\text{MAD}} \rightarrow -\infty$ and a linear taper in the field from r_{tr} to the ISCO so there is no initial magnetic flux any closer.

2.2 Numerical Grid and Density Floors

We use similar numerical grid mapping and identical boundary conditions as McKinney et al. (2012), except a smooth arctan transition from exponential to hyper-exponential radial grid spacing is used. For our high (mid) resolution grid we choose resolution $N_r \times N_\theta \times N_\phi = 192 \times 96 \times 208$ ($168 \times 64 \times 152$) with radial grid spanning $R_{\text{in}} \approx 0.75r_H$ (horizon radius r_H) to $R_{\text{out}} = 10^4 r_g$.

The θ -grid spans from 0 to π with the mapping of McKinney et al. (2012), but with $n_{\text{jet}} = 0$ used for our entire disk since it is thin at all radii. We adjust the constants of the mapping so that at $r/r_g = 6, 30, 100$ we resolve the disk vertically with 56, 62, 60 cells within $\pm 2H = 2 \cdot 0.1R$. We flare the inner radial grid to avoid unnecessarily small limiting time-steps. The polar boundary conditions are transmissive (see appendix in McKinney et al. 2012), and the ϕ -grid is equally spaced from 0 to 2π with periodic boundary conditions.

Apart from our direct resolution studies, we also measure convergence quality factors for the MRI and turbulence correlations lengths. Our values demonstrate good resolution and are reported in Section 3.5.

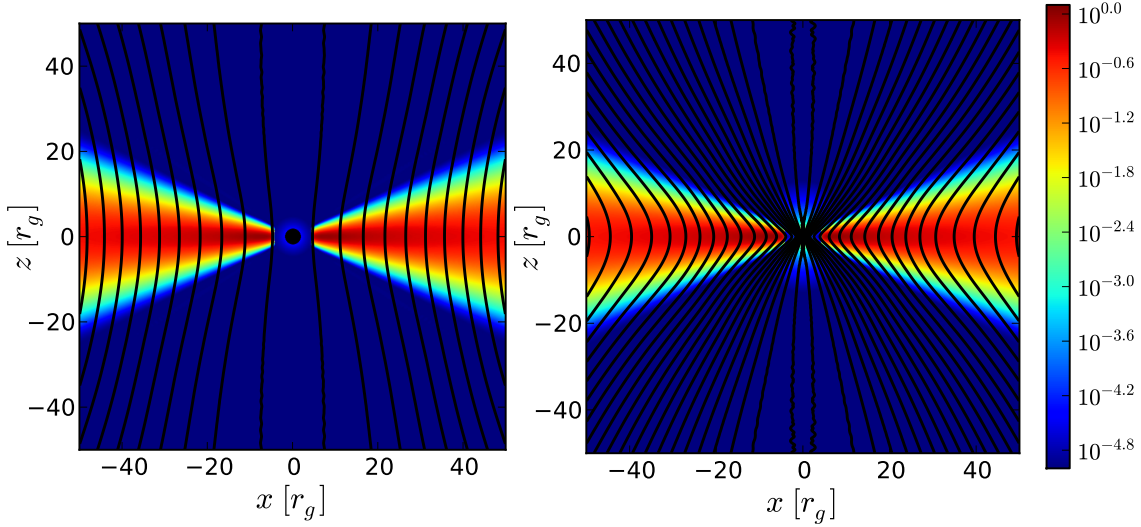


Figure 1. Snapshots of the initially sub-MAD (MADfHR - left panel) and nearly-MAD (MADiHR - right panel) models at $t=0$, showing ρ in color (with legend) with magnetic field lines (black lines). In MADfHR there is no magnetic field initially present within the ISCO or on the horizon and the field is weak throughout the disk. On the other hand, in MADiHR, a sufficient magnetic flux is present throughout the disk and on the horizon so that the disk will quickly become MAD out to large radius. The higher density surrounding the horizon in MADiHR at $t=0$ is the result of the density floor activated due to the presence of an initially strong magnetic field.

2.3 Cooling

To keep the disk thin and radiatively efficient, we implement an *ad hoc* cooling function similar to Noble et al. (2010) with

$$S_v = \left(\frac{dU}{d\tau} \right) u_v, \quad (2)$$

as a source term to the conservation equations, $\nabla_\mu T_v^\mu = S_v$, for gas stress-energy tensor T and 4-velocity u_v . This assumes an isotropic comoving rate of thermal energy loss $dU/d\tau$. dU is computed so that cooling decreases internal energy toward a target temperature set by the desired $H/R \approx 0.1$ and local density and radius.

Radiative cooling is efficient for a NT thin disk with a cooling timescale on the order of the orbital timescale (Novikov & Thorne 1973). The NT model assumes radiation gets out only by diffusion, while our disk is clumpy and can be optically thin near the ISCO (Zhu et al. 2012). Radiative GRMHD MAD simulations are required for an accurate cooling timescale, which could be faster than for literal NT disks (McKinney et al. 2015). We only try to keep the disk thin, and we settled upon a graded cooling timescale $d\tau$ so that

$$\frac{dU}{d\tau} = -\frac{\rho T_{\text{target}}}{d\tau} = -\rho T_{\text{target}} \cdot \begin{cases} \frac{\Omega_K/\tau_{\text{cool}}}{\frac{v_{\text{Alf}}}{H}} > \tau_{\text{cool}}/\Omega_K \\ \frac{v_{\text{Alf}}}{H} > \left(\frac{H}{v_{\text{Alf}}} \right) > 2\Delta t \\ \frac{1}{2\Delta t} & \left(\frac{H}{v_{\text{Alf}}} \right) < 2\Delta t \end{cases} \quad (3)$$

where v_{Alf} is the Alfvénic frequency and thus H/v_{Alf} is the Alfvén time across one disk scale height, $2\Delta t$ is the code time-step with a prefactor 2 for stability, and $\Omega_K = v_K/r$. The target temperature is from thin disk theory and is isotropic across cylindrical radii R ,

$$T_{\text{target}} \equiv \left(\frac{0.1 \cdot R}{a + r^{3/2}} \right)^2$$

where the denominator uses spherical radius r to control the temperature along the polar axes. If $T_{\text{gas}} = P_{\text{gas}}/\rho < T_{\text{target}}$ then $dU/d\tau = 0$. To ensure there is always rapid enough cooling, we set $\tau_{\text{cool}} = 0.1 \cdot 2\pi$ that enforces cooling on $1/10^{\text{th}}$ the orbital timescale.

We also use a temperature ceiling that acts as another cooling term, operating after each timestep. We limit the temperature where $\beta < 0.1$ and $T_{\text{gas}} > T_{\text{target}}$. Unfortunately these losses were not tracked in the version of HARM used. When we sum the radiative losses from the cooling function during our analysis, in order to compute the contribution lost to the temperature ceiling, we restarted MADiHR at a late time with the ceiling turned off. The additional heat is then captured by the cooling function which we can measure for the radii near the BH where the temperature ceiling mattered. Accounting for all cooling effects gives us a nearly constant radial profile for total efficiency, and so the procedure correctly recovers how a steady-state flow should behave.

Rest-mass density is injected whenever $2P_b/\rho > 200$ in order to ensure the code remains stable, and internal energy density is added when $e_{\text{gas}}/\rho > 100$ (though this limit is never reached).

As seen in Fig. 5 the cooling keeps the disk very close to the target scale height. After a very short ($< 5000r_g/c$) initial period of disk evolution, the disk height is very stable.

2.4 Diagnostics

The disk's geometric half-angular thickness (H) per radius (R) is

$$\frac{H}{R}(r, \phi) \equiv \frac{\left(\int_{\theta} \rho(\theta - \theta_0)^n dA_{\theta\phi} \right)^{1/n}}{\left(\int_{\theta} \rho dA_{\theta\phi} \right)^{1/n}}, \quad (4)$$

where

$$\theta_0(r, \phi) \equiv \frac{\pi}{2} + \frac{\left(\int_{\theta} \rho(\theta - \pi/2)^n dA_{\theta\phi} \right)^{1/n}}{\left(\int_{\theta} \rho dA_{\theta\phi} \right)^{1/n}}, \quad (5)$$

and with surface differential $dA_{\theta\phi}$. Typically we use $n = 1$ but also compare to using other n .

The radiative energy and angular momentum lost are

$$L_v(r) = \int R_v'(r) dA_{\theta\phi} = -\frac{1}{Dt} \int_{D_t} \int_{R_{\text{cap}}}^r S_v dt dV, \quad (6)$$

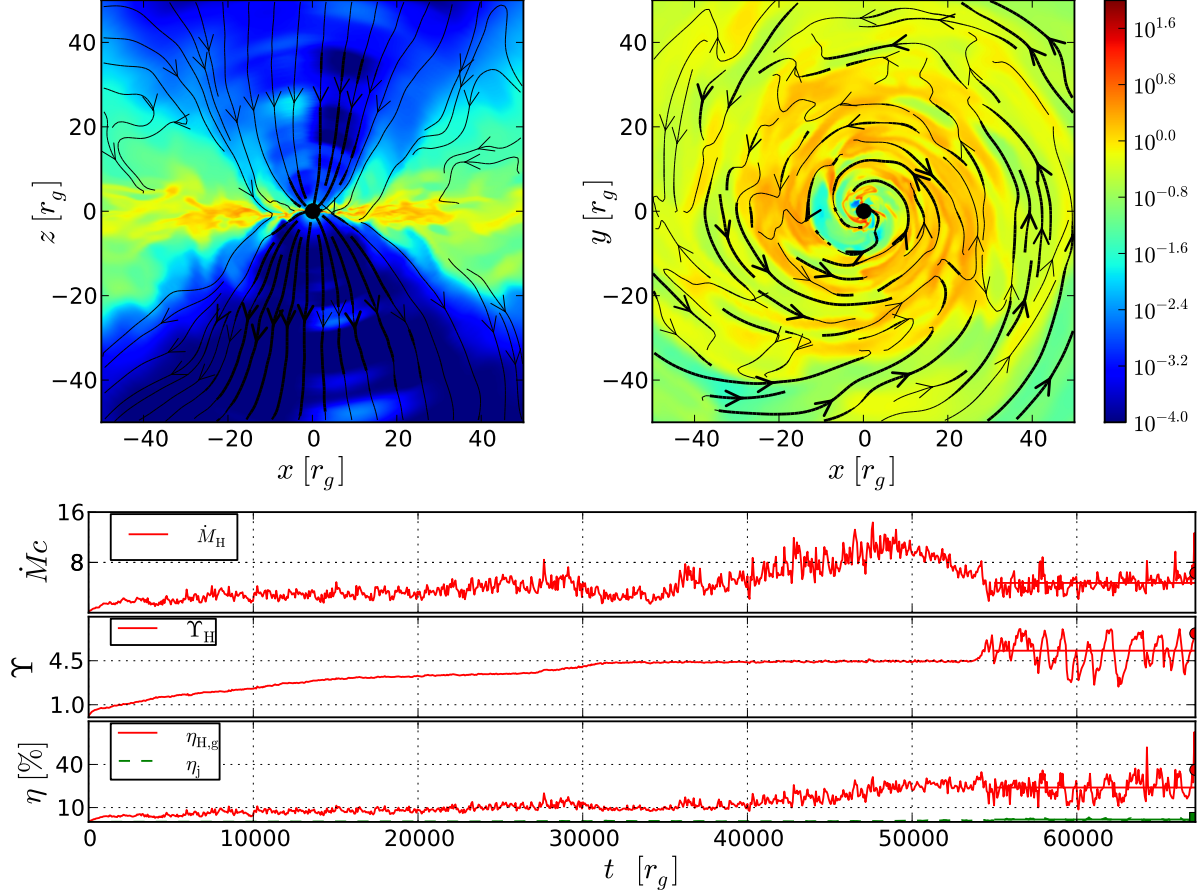


Figure 2. Evolved snapshot of the MADfHR model at $t \approx 70,000 r_g/c$ showing log of rest-mass density in color (with legend) in both the $z-x$ plane at $y=0$ (top-left panel) and $y-x$ plane at $z=0$ (top-right panel). Black lines with arrows trace field lines, where thicker black lines show where field is lightly mass-loaded. The bottom panel has 3 subpanels. The top subpanel shows the mass accretion rate through the BH (\dot{M}_H). The middle subpanel shows the magnetic flux threading the BH (Υ_H), normalized so that order unity is a dynamically-substantial amount of magnetic flux. The bottom subpanel shows the gas efficiency measured on the horizon ($\eta_{H,g}$) and jet efficiency measured at $r=50r_g$ (η_j). In this model, the disk initially has a weak large-scale poloidal magnetic field, which is transported by the MRI and other magnetic stresses toward the BH. Eventually, by $t \sim 55000 r_g/c$, the magnetic flux saturates on the BH and cannot grow despite plentiful magnetic flux outside. The MAD state that develops consists of a highly non-axisymmetric clumpy thin disk with a weak ($\eta_j \sim 1\%$) jet.

respectively, for $v = t, \phi$ for some period Dt over all angles with photon capture radius R_{cap} (see §3). The radiation contribution from beyond the inflow equilibrium radius ($\sim 30r_g$ for our MADiHR model) is conservatively estimated by using NT’s radial dependence.

The mass accretion rate, energy efficiency, and specific angular momentum accreted are, respectively,

$$\dot{M} = \left| \int \rho u^r dA_{\theta\phi} \right|, \quad (7)$$

$$\eta = -\frac{\int (T_t^r + \rho u^r + R_t^r) dA_{\theta\phi}}{[\dot{M}]_H}, \quad (8)$$

$$J = \frac{\int (T_\phi^r + R_\phi^r) dA_{\theta\phi}}{[\dot{M}]_H} \quad (9)$$

where R is the radiation stress-energy tensor and $[\dot{M}]_H$ is the time-averaged \dot{M} on the horizon. These quantities are calculated as totals and for the jet and wind. The jet is defined as where $2P_b/\rho > 1$, and the wind is where $2P_b/\rho < 1$ with an outgoing flow. The radiative efficiency and specific angular momentum vs. radius are, respectively, $\eta_r = -L_r(r)/[\dot{M}]_H$ and $J_r = L_\phi(r)/[\dot{M}]_H$.

The dimensionless magnetic flux, that measures the strength of the magnetic field threading the BH or disk, is

$$\Upsilon(r) \approx 0.7 \frac{\int dA_{\theta\phi} 0.5|B^r|}{\sqrt{[\dot{M}]_H}}, \quad (10)$$

for radial magnetic field strength B^r in Heaviside-Lorentz units, where Υ_H is Υ measured on the horizon and

$$\Psi(r) = \int dA_{\theta\phi} 0.5|B^r|$$

is the radial absolute flux passing through a given radius.

Viscous theory gives a GR α -viscosity estimate for v_r , of $v_{r,\text{visc}} \sim -G\alpha(H/R)^2 |v_\phi|$, as defined in McKinney et al. (2012), leading to a definition for the measure of effective α -viscosity

$$\alpha_{\text{eff}} \equiv \frac{v_r}{v_{\text{visc}}/\alpha}, \quad (11)$$

whereas viscosity from local shear-stress in the disk is

$$\alpha_b \approx \alpha_{\text{mag}} = -\frac{b_r b_\phi}{p_b}, \quad (12)$$

where we have dropped other (e.g. Reynolds) terms from the full α

because they are negligible compared to the magnetic term in the MAD regions of our simulations. These α 's (see Fig. 9) are obtained by separately volume-averaging the numerator and denominator in θ, ϕ for each r with a weight of ρ and only including material with $b^2/\rho_0 < 1$ in order to focus the measurement on the disk material and not the lower density corona. The quantity α_b measures the magnetic stress within the dense regions, while the $\alpha_{b,\text{eff}}$ measures the actual effective α based upon the radial velocity of the dense regions. For example, very little magnetic flux may thread the dense regions, but external magnetic torques may push and drive angular momentum transport and inflow of the dense regions. $\alpha_{b,\text{eff}}$ is only accurate far outside r_{ISCO} because of the G term.

3 RESULTS AND DISCUSSION

With our fully global 3D GRMHD simulations we can demonstrate whether the non-linear MRI and other MHD physics in thin accretion flows is able to transport large-scale magnetic flux towards the BH and build-up the magnetic field to the MAD state. We first consider a disk with a weak magnetic field using our MADiHR setup to see if magnetic flux transports inward. Then, having confirmed thin disks transport magnetic flux efficiently to the BH and inner-radial disk, we use our second setup MADiHR to study a MAD where magnetic saturation is reached to large radii. This two-step procedure is necessary due to the extreme computational resources that would otherwise be necessary to build-up large-scale flux to the MAD state out to large radii.

3.1 Demonstration of flux accumulation to MAD state

First, we consider a thin radiatively efficient disk threaded by weak large-scale magnetic field. This model, MADfHR/MR, started in the sub-MAD state with $\beta \approx 200$ (a field strength that is ~ 7 times weaker than when the MRI is suppressed and ~ 40 times weaker than the final MAD state) so that the MRI operates over long times. In MADfHR the MRI leads to accretion of magnetic flux inward, such that over $t \approx 70,000 r_g/c$ the BH and disk become MAD out to $r \sim 15 r_g$. Fig. 2 shows a steady accumulation of flux during the first $\sim 30000 r_g/c$. The level of flux then remains constant on the horizon for another $\sim 20000 r_g/c$ due to an excess of rest-mass accumulating in the inner disk that slowly accretes. This denser torus forms as the magnetic flux threading the inner section of the disk accretes onto the BH during the early evolution and temporarily starves some disk material of strong field. The local viscosity is then suppressed until magnetic flux from further out in the disk has time to transport inward. Once this initial dense torus accretes, the disk enters a MAD regime of accretion.

In the much longer run, MADfMR becomes MAD out to a radius of $r \sim 18 r_g$ by the time $t \approx 183,000 r_g/c$. Plenty more magnetic flux exists at larger radii, but it would presumably contribute to the MAD region of the disk at later times. The physics of magnetic flux accumulation involves the weak field MRI driving accretion, magnetic braking via the wind transporting material and magnetic flux inward, and may involve the field penetrating coronal-like material in the disk (e.g., see Rothstein & Lovelace 2008; Beckwith et al. 2009). At early times, magnetic flux at higher latitudes transport more readily than those in the equator, but eventually magnetic flux threading the disk is also transported to the region close to the BH. Whatever is the physics behind the saturation of magnetic flux, it has reached a maximum far below the supply, yet far beyond the initial value. This demonstrates that large-scale magnetic flux can

readily accumulate even with $H/R \approx 0.1$ and radiative cooling, and that it reaches a saturated value like seen in prior MAD simulations.

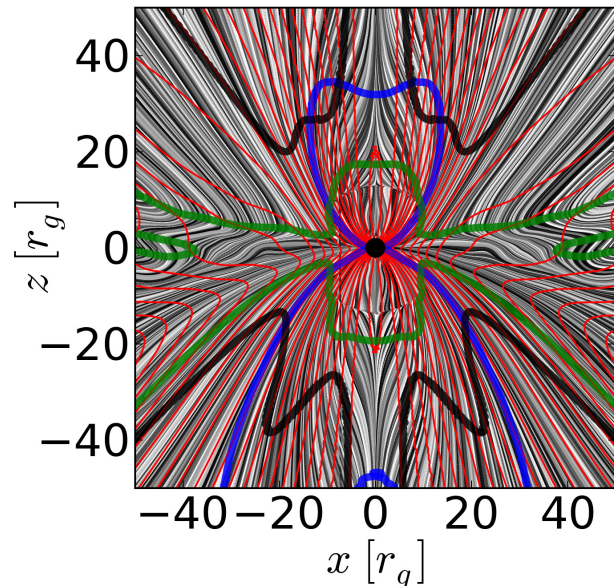


Figure 3. Time and ϕ -averaged quantities are plotted for MADfHR. Rest mass gas flow is traced by black streamlines. The colored (green, black, and blue) thick lines correspond to time-averages of quantities $Y = \{u', u_r, b^2/\rho_0\}$, respectively, at values $[Y]_t = \{0, -1, 1\}$. While near the BH the flow has $[b^2/\rho_0]_t \geq 1$ as averaged directly, the dense inflow has $[b^2/\rho_0]_t \leq 1$ at all other radii. Streamlines nearest the polar axes are calculated using velocity structure five cells away from the axis for better visualization of the qualitative geometry of the jet flow. The flow exhibits equatorial asymmetry over many inflow times as found in thicker MAD simulations. The red magnetic field line contours show how the magnetic flux threads the black hole and inner disk.

Fig. 3 shows the time and ϕ -averaged rest-mass velocity streamlines as well as several key boundaries associated with the accretion flow. This includes showing the jet boundary and the flow stagnation surface (where material has zero radial velocity, moves outward at higher latitudes, and moves inward at lower latitudes). Most importantly, the plot indicates the time- ϕ -averaged structure of the magnetic field once the inner disk and BH have reached magnetic flux saturation. As with the thicker MAD model plotted similarly in Fig. 6 of McKinney et al. (2012), the time- ϕ -averaged steady-state field structure, as well as the evolution we see in movies, demonstrate ordered poloidal magnetic flux is easily transported through the disk from large radii.

3.2 Long-term evolution of MAD state

In order to study the thin MAD out to large radii to ensure an accurate quasi-steady radiative efficiency, we next considered the disk having an initially nearly MAD-level of magnetic field. Fig. 1 and Fig. 4 show the initial and evolved quasi-equilibrium state of our high-resolution model that is initially nearly MAD inside $r = 30 r_g$. As the accretion flow evolves from its initial state, rotation drives outward angular momentum transport by turbulent magnetic stresses via the MRI as well as by a wind. Mass, energy, angular momentum, and magnetic flux are accreted and ejected, and by $\sim 5000 r_g/c$ magnetic stresses balance incoming gas forces so

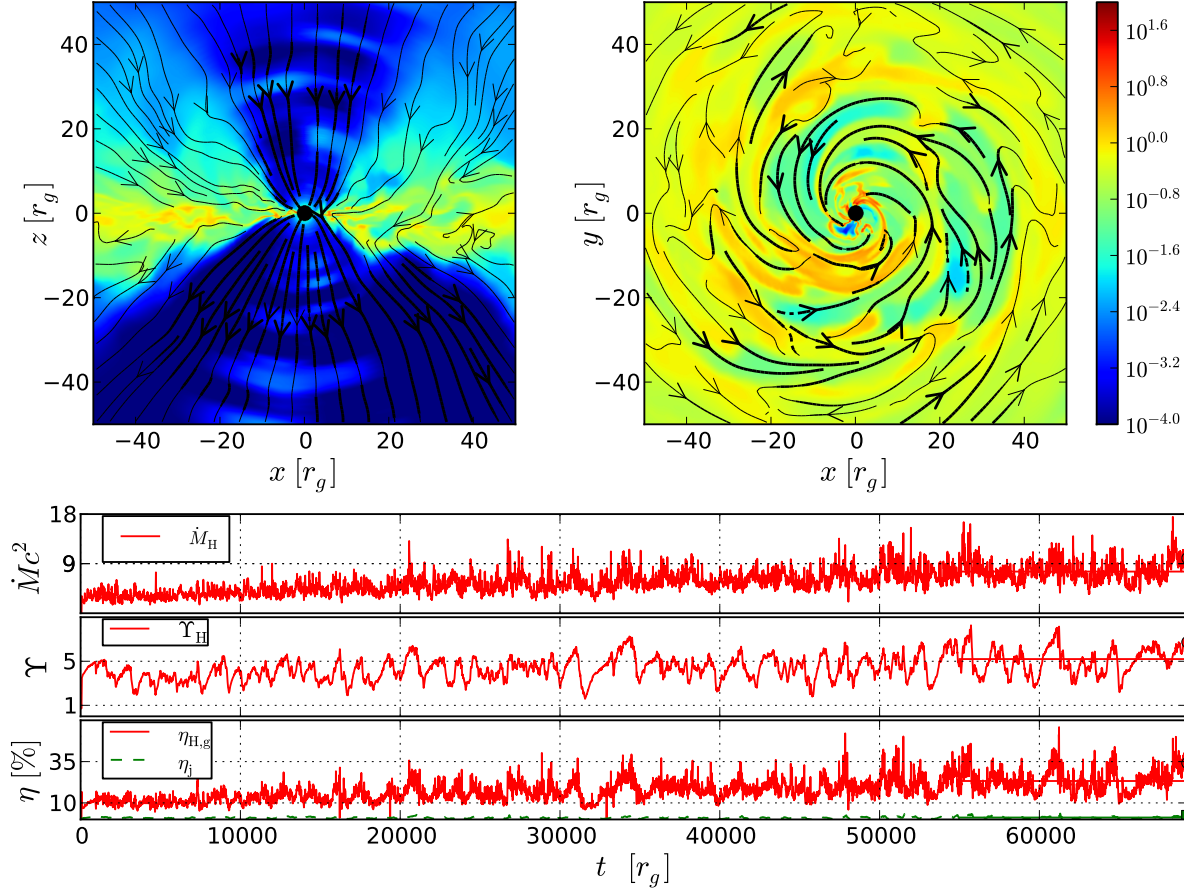


Figure 4. Evolved snapshot of the MADiHR model at $t \approx 70,000 r_g/c$, with identical layout to Fig. 2. The MAD state is highly non-axisymmetric and clumpy with a weak ($\eta_j \sim 1\%$) jet. The rest-mass accretion rate and magnetic flux on the horizon reach the MAD state quickly, which was as desired so that we can study a quasi-steady MAD out to large radii over long time periods. The dimensionless magnetic flux on the horizon is in agreement with our MADfHR model, showing a disk initial condition with a relatively stronger poloidal field strength still reaches the same MAD state near the BH.

the accretion is MAD out to $r \sim 30 r_g$. By the end of the simulation, $t \sim 70000 r_g/c$ for MADiHR, the MAD extends to $r \sim 35 r_g$.

The evolved state is evaluated using the period $t = [30000, 70000] r_g/c$ for time-averaging quantities. A slightly longer period $t = [10000, 70000] r_g/c$ is used for the time-averaged functions of radius in Fig. 5 to minimize the effects of long-term trends. The time- ϕ -averaged structure is shown in Fig. 7 and shows qualitatively similar behavior to MADfHR.

The gas+radiative efficiency $\eta \sim 20\%$, and specific angular momentum $j \approx -0.4$ are constant within the MAD/non-MAD transition $r \sim 35 r_g$, indicating a quasi-steady MAD state has been reached out to a relatively large radius.

The disk thickness at $r \sim 20 r_g$ is regulated by cooling to be $H/R \approx 0.11$ for $n=1$ in Eq. 4, $H/R \approx 0.14$ for $n = 2$, density-weighted normalized $H/R \approx 0.13$ (Penna et al. 2012), and thermal thickness of $\bar{h} \equiv \arctan(c_s/v_{\text{rot}}) \approx 0.13$. An accurate measurement of H/R is complicated by the fact that magnetic compression leads to a geometric $H/R \approx 0.05$ near the BH, mass is launched into a broad wind, and vertical disk fluctuations are the same order as H/R . For the ϕ -averaged density profile and including only bound material (i.e. $-u_r(\rho + e_{\text{gas}} + P_g + 2P_b)/\rho < 1$), valid when comparing with NT, we get $H/R \approx 0.10$, which is our target value we desired for the disk proper. Fig. 6 shows the time evolution of H/R at four radii for $n = 1$.

Our thin MAD achieves a magnetic flux on the BH of $\Upsilon_H \approx 5$.

The stability of Υ_H with time and the presence of plentiful magnetic flux remaining in the disk (see Fig. 6, lower panel) indicate that the disk has achieved a balance between magnetic forces and gas forces with a strong magnetic field ($\Upsilon \gg 1$). Thus one expects maximum magnetically-induced deviations from the standard NT thin disk solution.

Large temporal deviations are driven by magnetic flux repeatedly building up on the BH horizon to a level the disk cannot sustain. As soon as a weak point in the density exists caused by a non-axisymmetric mode, then there is a sudden re-emergence of magnetic flux back into the disk, a process that creates large low-density bubbles in the form of a magnetic prominence. The magnetic flux that is ejected is then processed by turbulence by the outer parts of the disk until being accreted again at which point the process repeats. Fig. 8 shows one of the most extreme magnetic prominences occurring in the MADiHR simulation.

3.3 Radiative Efficiency

We find that nearly as much radiation is released near and inside the ISCO as in the entire rest of the disk, so we calculate the radiative efficiency assuming 100% photon capture within a choice among three radii: the horizon, the photon orbit radius $r \approx 2.4$, and the critical impact parameter radius, $r \approx 4.1$, for which geodesics with any smaller impact parameter intersect the horizon. An estimate of

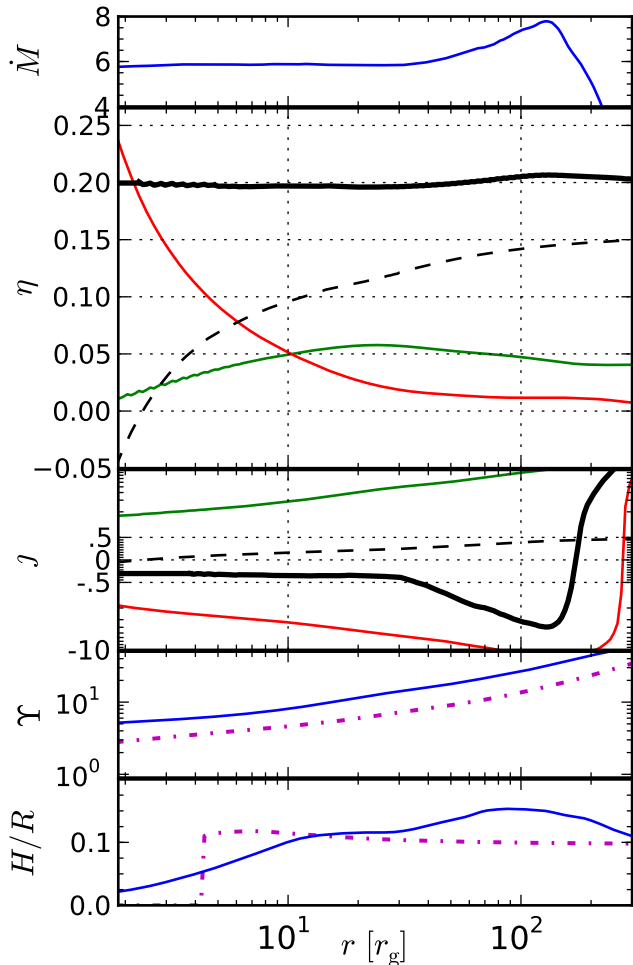


Figure 5. Time-averaged quantities as a function of radius. From top to bottom, panels are: Total mass accretion rate (\dot{M} , blue line), energy efficiency (η), specific angular momentum (j), magnetic flux (Υ), and disk thickness (H/R , $n=1$ in Eq. 4, blue line). Plots for η and j show total gas+radiative (black solid), electromagnetic (green), matter (red), and radiation (black dashed) components. Remaining plots show their initial value (magenta dot-dash). The plot of Υ shows that for the total BH+disk contribution (blue). The constancy of \dot{M} , η , j show where the flow has achieved inflow equilibrium. Υ shows the MAD to non-MAD transition at $r \sim 35r_g$, while throughout the disk $H/R \approx 0.1$ (bound gas), as maintained by cooling. The primary result of this plot is the efficiency panel showing the radiative contribution of $\eta_r \sim 15\%$ with most of emission beyond the standard NT disk model coming from quite close to the photon orbit.

photon capture using ray-tracing from a thin disk (see Beckwith et al. 2006) gives as much as 30% escape fraction from the photon orbit for equivalent BH spin, and more than 70% for $r \approx 4.1$. This suggests using the photon orbit may give the best, simplest approximation.

The radiative efficiency is $\eta_r \sim 15\%$ for MADiHR ($< 0.5\%$ lower for MADiMR) when including only radiation from outside the photon orbit. This is about twice larger than the $\eta_r \approx 8\%$ efficiency in standard NT thin disk theory for BH spin $a/M \approx 0.5$. The impact parameter estimate is an extreme, albeit unphysical, limit giving efficiency $\eta_r \sim 9.4\%$. Also unphysical, including all radiation released outside the horizon gives $\eta_r \sim 19\%$. Unbound gas only contributes $\sim 1\%$ to η_r , a smaller relative contribution compared to prior simulations (Penna et al. 2010; Zhu et al. 2012).

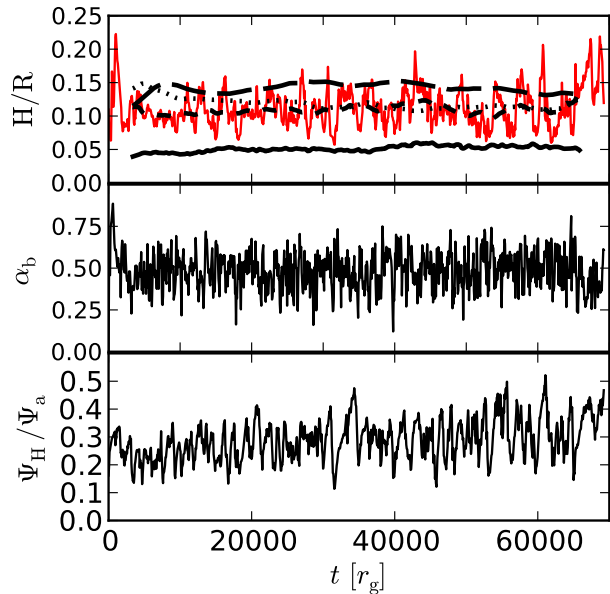


Figure 6. Shows temporal evolution of a few quantities for our MADiHR model. The disk scale height H/R is shown in the top panel. We show the temporally-smoothed H/R as plotted for radii R_{ISCO} (solid-black), $15r_g$ (short-dashed), $30r_g$ (dots), and $60r_g$ (long-dashed). The red line is the unsmoothed evolution at $15r_g$ to demonstrate the level of variability. The H/R value is regulated by cooling to be $H/R \sim 0.1$, which is what is achieved for radii just outside the ISCO and out to the inflow equilibrium radius of $r \sim 35r_g$. The middle panel shows the α_b viscosity parameter spatially-averaged over the disk at a radius $10r_g$. The relatively high $\alpha_b \sim 0.5$ is indicative of MADs, implying efficient transport of mass and angular momentum. The third panel shows the ratio of the total magnetic flux threading the BH to the total magnetic flux available at the start of the simulation inside the radius out to which the simulation ultimately reaches at least one inflow time. This shows that the horizon contains much more magnetic flux than is available, so the quasi-steady state has a horizon-threading flux that has reached saturation.

Thus, our thin MAD with $H/R \approx 0.05\text{--}0.1$ and a radiative efficiency of $\eta_r \approx 15\%$, demonstrates an $\approx 80\%$ deviation from NT. Prior GRMHD simulations of thin disks have had $H/R \approx 0.1$ with 6% deviations (Noble et al. 2009), $H/R \approx 0.06$ with 6% to 10% deviations (Noble et al. 2011), and $H/R \approx 0.07\text{--}0.13$ with 4% to 5% deviations (Penna et al. 2010). So despite having similar H/R , our thin MAD has vastly higher deviations from NT.

3.4 Jet Efficiency

Some of the horizon magnetic flux reaches into the polar regions leading to a jet efficiency of $\eta_j \approx 1\%$ at $r = 50r_g$ for both MADiHR and MADfHR. A caveat is that the jet within $b^2/\rho_0 > 1$ at $r = 50r_g$ is only resolved by about 7 grid cells. So we check the jet efficiency and resolution on the horizon, where the jet is resolved with more than 12 grid points per hemisphere and still has a jet power of $\eta \approx 1\%$. These horizon jet grid cells are sufficient resolution to capture the force-free behavior of the jet near the polar axes, according to prior resolution studies (McKinney & Gammie 2004). So the jet efficiency measurement is robust to resolution changes, slight model changes, and what radius it is measured at.

The BH spin and disk rotation drive a magnetized wind with efficiency $\eta_w \approx 4\%$, though at least an additional 1% wind efficiency may be lost to radiation via the very efficient cooling we use

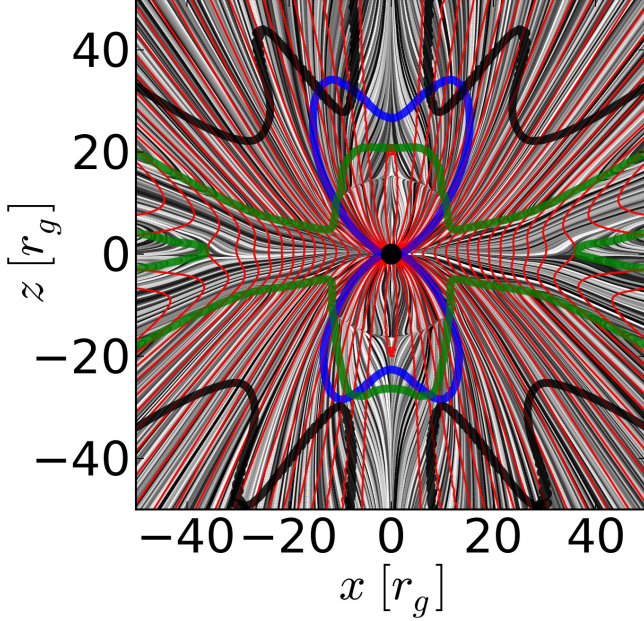


Figure 7. Time and ϕ -averaged quantities are plotted for MADiHR. Identical layout as Fig. 3. The disk is magnetically arrested out to a transition radius of $\sim 35r_g$, which leads to a short inflow time-scale compared to the MADfHR disk at those radii, so the time-averaged velocity fields and other disk structure is smoother and more symmetric.

as well as lost to the comparatively low ω resolution in the jet and highly magnetized wind regions.

The jet and wind contribute only a bit to the total $\eta \approx 20\%$. However, the jet and wind carry nearly as much angular momentum outward as the dense Keplerian disk carries inward. This results in the BH spin-up parameter $s = -j - 2(a/M)(1 - \eta) \approx -0.4$, i.e. somewhat spinning down (McKinney et al. 2012).

Further, the jet efficiency as a function of H/R is constrained by our thin MAD result. Magnetic compression leads to varying geometric H/R vs. radius, so the more constant thermal thickness $\bar{h} \equiv \arctan(c_s/v_{\text{rot}})$ is used (McKinney et al. 2012). Our thin MAD models have $\bar{h} \approx 0.13$ and older MADs had $\bar{h} \approx 0.5$ (e.g. with geometric $H/R \approx 0.3$ at $r = 20r_g$) or $\bar{h} \approx 1.5$.

Prior thick MAD simulations found that the saturated magnetic flux on the BH given by Υ is roughly constant vs. BH spin. That data showed a slight tendency to peak at $a/M \sim 0.5$, but this is probably intrinsic to the initial disk conditions or due to intrinsic errors that suggest $a/M \sim 0$ could be the peak as well (McKinney et al. 2012; Tchekhovskoy et al. 2012). The thick MAD simulations of moderate thickness show a clear asymmetry in the Υ vs. spin for positive vs. negative spin that is consistent with the asymmetry in jet efficiency vs. spin. So we do not try to fit the peak in Υ being at $a/M \sim 0.5$, but we capture the asymmetry. We also capture the fact that this spin asymmetry is seen to go away as the disc becomes even thicker.

Combining the different thick MAD models with our new thin MAD model, a rough fit of the jet power is given by

$$\eta_j \sim 400\% \omega_H^2 \left(1 + \frac{0.3\omega_H}{1 + 2\bar{h}^4} \right)^2 \bar{h}^2, \quad (13)$$

where $\omega_H \equiv a/r_H$, which assumes steady activation of a Blandford & Znajek (1977) jet. The $\eta_j \propto \bar{h}^2$ scaling is required (compared to $\propto \bar{h}$) to reach our thin MAD with $\eta_j \approx 1\%$. That $\eta_j \propto (H/R)^2$ is

consistent with S7.1 of Penna et al. (2010) who analytically found $\Upsilon \propto (H/R)$, and with Meier (2001) who argued that $\eta_j \propto (H/R)^2$.

This formula is roughly consistent with what is expected based upon the BZ formula $\eta_j \propto \Upsilon^2 \Omega_H^2$. Models with $\bar{h} \approx 0.5$ and $a/M = 0.5$ gave $\eta_j \sim 20\%$ and $\Upsilon \approx 13$. Our thin MAD has $\Upsilon \approx 5$, so the BZ formula suggests we should get $\eta_j \approx 3\%$ while we got $\eta_j \approx 1\%$. Why the factor of three difference?

First, Υ measured on the BH is not relevant to the BZ jet. One cannot use Υ_H with $\eta_j \propto \Upsilon_H^2$, because in general (and as found in thicker MAD models) magnetic flux in the jet is a fraction of Υ_H and the jet only partially covers the rotating BH's surface. Instead, the magnetic flux passing through the jet is what is relevant to the jet power. The $\bar{h} \approx 0.5$ model had $\Upsilon_j \approx 10$, while our model has $\Upsilon_j \approx 4$. These are significantly different from the magnetic flux over the entire horizon. This still implies we should have $\eta_j \approx 3\%$ for consistency with the BZ expectation.

Second, the BZ formula fails to account for the disk covering a significant part of the potential power output (McKinney 2005). The disk at the equator gets in the way, even for MADs (especially at lower spin when less magnetic compression occurs). However, most of the BZ power would be at the equator where the Poynting flux peaks. The disk chops-off this peaked part of the Poynting flux for the jet, giving some of it to the wind. Some of that BZ power is never produced in the first place due to the heavy mass-loading by the disc. A better model of that disk part that connects to the horizon is the Gammie (1999) model of a thin magnetized disc. In that case, Υ locally in the disk is much less than over the entire horizon, so the Gammie (1999) model predicts much less than BZ for extraction of energy. One cannot just fit η_j vs. Υ_H and expect it to match BZ.

Third, we have defined the jet arbitrarily as where $b^2/\rho_0 > 1$. The wind is defined as the rest of the non-radiative flux that adds up to the total efficiency. For our thin MAD, this is 4% (i.e. 20%-1%-15%). The wind efficiency is partially directly due to the disk rotation, but some of the wind efficiency derives from magnetic flux threading the BH that passes into the disk leading to a BH-spin-driven wind. Some of this BH-spin-driven wind absorbs what would have otherwise (without a disk) become the jet and can account for another missing 2%, giving a total BZ-like efficiency matching expectations. If this were the sole effect in comparison to the thicker MAD models, this would suggest that thin MADs may have more powerful winds per unit jet power relative to thick MADs.

Fourth, the jet efficiency for the $\bar{h} \approx 0.5$ $a/M = 0.5$ model is a peak among all the otherwise identical models with different BH spins. Given how much the results vary for slight changes in the model setup (like initial magnetic field strength), the $\eta_j \approx 20\%$ could easily have been $\eta_j \approx 10\%$ within systematic errors. Then there would be no discrepancy between our formula and the BZ approximation.

So our Eq. (13) is not supposed to be derived from BZ because the BZ-driven process creates both a “jet” and a “wind”, while we have defined the jet by that part which would be capable of becoming relativistic. So in that sense, our formula is useful in application to real jets instead of a test of whether the theoretical BZ extraction efficiency applies to the simulation data. However, only direct observational comparisons without ad hoc definitions will test the validity of these simulations being applicable to real systems. The fitting formula is just a useful guide.

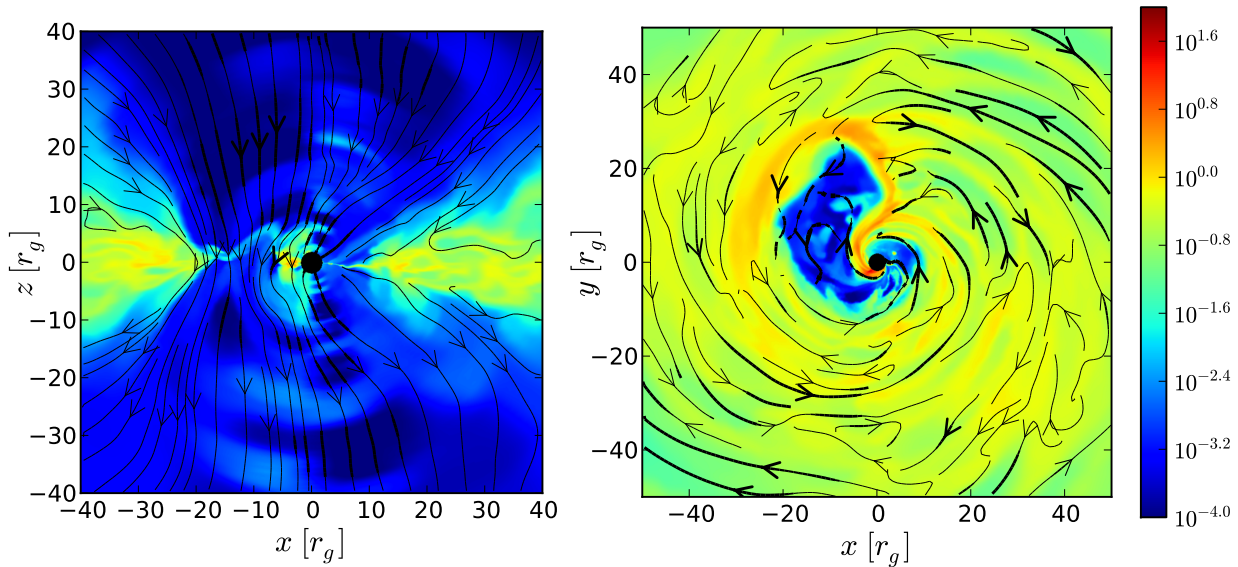


Figure 8. Plotted as in the top frames of Fig. 4 is a snapshot of MADiHR at $t = 31568 r_g / c$ when the disk experiences an extreme eruption of magnetic flux from the BH horizon. A large magnetic flux tube creates a low-density cavity in the disk before it is partially blended with disk material by the magnetic Rayleigh-Taylor instability. Such prominences occur frequently in the MAD state.

3.5 Resolution

We test the resolution of our simulations using convergence quality factors for the MRI ($Q_{\theta\phi, \text{MRI}}$; number of grid cells per MRI wavelength in each direction) and turbulence ($Q_{r\theta\phi, \text{corr}}$; number of cells per turbulence correlation length in each direction) (Shiokawa et al. 2012; Hawley et al. 2011; McKinney et al. 2012; Hawley et al. 2013; McKinney et al. 2013, 2014). For our high resolution runs, MADiHR (MADfHR), at $r = 12, 30 r_g$ centered on the equatorial flow, we have $Q_{\theta, \text{MRI}} = 160, 55$ ($Q_{\theta, \text{MRI}} = 88, 18$) with a weighting of $\sqrt{\rho b^2}$ and we have $Q_{\phi, \text{MRI}} = 120, 100$ ($Q_{\phi, \text{MRI}} = 79, 77$) with a weight of ρ . Weighted averages are computed for the numerator and denominator separately before taking the ratio to get Q . The purely density-weighted values represent a stricter constraint on whether we have sufficient resolution (because MADs have strong fields mostly outside the dense region, and the external stresses are important to whether transport occurs), and these are plotted as a function of radius in Fig. 9. Resolution of rest-mass and magnetic energy densities are evaluated at four radii $r = \{r_H/r_g, 4, 8, 30\} r_g$. For MADiHR, rest-mass correlation values are, at each radius respectively, $Q_{r, \text{corr}} \sim 6, 10, 14, 14$, $Q_{\theta, \text{corr}} \sim 40, 35, 31, 34$, and $Q_{\phi, \text{corr}} \sim 6, 7, 8, 11$. Correlation values for magnetic energy density are, similarly, $Q_{r, \text{corr}} \sim 6, 12, 17, 15$, $Q_{\theta, \text{corr}} \sim 34, 33, 29, 36$, and $Q_{\phi, \text{corr}} \sim 8, 9, 12, 16$.

For MADfHR, calculated for the disk once the BH has reached the MAD state, rest-mass correlation values are, at each radius respectively, $Q_{r, \text{corr}} \sim 6, 10, 14, 14$, $Q_{\theta, \text{corr}} \sim 3, 29, 28, 32$, and $Q_{\phi, \text{corr}} \sim 7, 9, 11, 13$. Correlation values for magnetic energy density are, similarly, $Q_{r, \text{corr}} \sim 6, 12, 16, 15$, $Q_{\theta, \text{corr}} \sim 5, 28, 30, 31$, and $Q_{\phi, \text{corr}} \sim 7, 9, 12, 14$.

These MRI and turbulent quality factors are high enough to ensure the reported simulations are resolving all the necessary turbulent physics and are likely converged. We also directly convergence tested our results by performing simulations of each setup with three resolutions. The qualitative structure of the disk in the MR and HR simulations are the same, but the lower resolution in

MR allowed us to run these simulations for significantly longer. The nature of magnetic flux accumulation is the same, but the longer MR simulations become magnetically arrested to larger radius, $r \sim 18 r_g$ in MADfMR compared to only $r \sim 15 r_g$ in MADfHR. A difference of only $\sim 0.5\%$ in radiative efficiency between MADiMR and MADiHR indicates very good convergence in our quantity of interest. We find only small (typically $\sim 10\%$ or less) differences between our MR and HR simulations for the other quantities reported which characterize the accretion flow. For instance, the jet power differs by only $\sim 50\%$ between MADiMR and MADiHR, unsurprising since $\Upsilon \approx 5$ for both. Low resolution ‘testing’ simulations were largely in qualitative agreement, but with some Q 's indicating lack of convergence.

Figs. 6 and 9 show values of the α_b viscosity parameter, dominated by the magnetic stress. We find $\alpha_b \sim 0.5$, as consistent with resolved disks in prior MAD simulations. The effective viscosity $\alpha_{b, \text{eff}}$, corresponding to a measurement of the actual inflow rate indicated by an α parameter, is much larger than α_b due to enhanced inflow caused by external torques driven by low-density highly-magnetized material that introduces large-scale stresses on the more dense inflow.

3.6 Power-law Fits for Radial Dependence

We now consider radial power-law fits (of the form $f = f_0(r/r_0)^p$) for quantities associated with the disk structure and flow, plotted in Fig. 10, for MADiHR. The fits to disk quantities are performed as in McKinney et al. (2012) between radii $r = 12 r_g$ and $r = 30 r_g$ for both our high resolution models. The profiles for MADiHR (MADfHR) are $\rho_0 \propto r^{-0.4 \pm 0.1}$ ($\propto r^{-0.8 \pm 0.2}$), $p_g \propto r^{-1.5 \pm 0.1}$ ($\propto r^{-1.8 \pm 0.1}$), $|v_r| \propto r^{-1.6 \pm 0.06}$ ($\propto r^{-0.8 \pm 0.2}$), $|v_\phi| \propto r^{-0.38 \pm 0.01}$ ($\propto r^{-0.49 \pm 0.01}$), $|b_r| \propto r^{-1.4 \pm 0.07}$ ($\propto r^{-1 \pm 0.1}$), and $|b| \propto r^{-1.2 \pm 0.05}$ ($\propto r^{-0.89 \pm 0.02}$).

The MADiHR fits are more representative of a steady-state MAD solution, because the disk in MADiHR is actually magnetically arrested over all radii used for fitting and the model is in

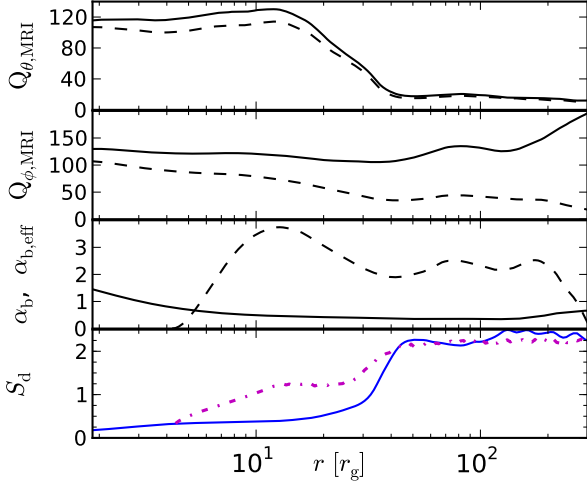


Figure 9. MRI quality factors indicating time- ϕ averaged resolution, viscosity of the disk, and vertical MRI half-wavelengths per disk scale height (S_d , blue line) are plotted as a function of radius. Q factors indicated the number of grid cells per critical MRI wavelength, averaged with weight $\sqrt{\rho b^2}$ (solid lines) and ρ (short dashed) across the disk where $b^2/\rho < 0.5$. The third panel shows the viscosity parameter α_b (solid line) and the effective viscosity calculated via the mass accretion rate (short dashed). The magnetic evolution of the disk is well resolved and leads to a high viscosity as measured by local stresses, α_b , and the rate of mass inflow $\alpha_{b,\text{eff}}$. The magenta dot-dash line represents the value of S_d at $t=0$ and the time-average is blue-solid.

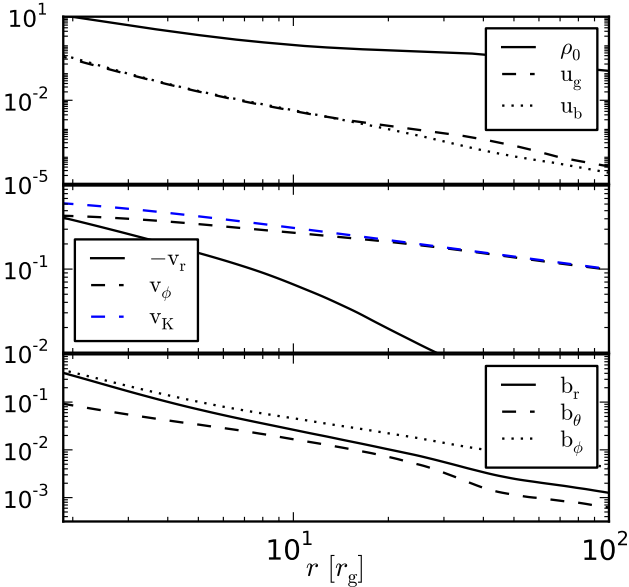


Figure 10. Several quantities characterizing the accretion flow in MADiHR are plotted as a function of radius. The top panel shows the density profile ρ_0 (solid), the internal gas energy u_g (dashed), and magnetic energy density u_b (dotted). The inner disk, that has reached the MAD state, has $u_g \sim u_b$ indicating equipartition is achieved even within the dense parts of the disk. The middle panel includes the disk radial velocity, azimuthal velocity, and Keplerian velocity (v_r , solid; v_ϕ , black-dashed; v_K , blue-dashed, respectively). The final panel shows the radial profiles of each component of the comoving magnetic field, $b_{r,\theta,\phi}$, in solid, dashed, and dotted lines respectively. The density is shallower than thicker disk solutions, the disk is fairly Keplerian, and the magnetic field falls off as expected for accretion disks.

inflow equilibrium out to large radii. Our thin disk has a somewhat shallower radial density profile than prior MAD models, but are otherwise consistent. To obtain a density profile accurate to large radii, much longer-run simulations would be required. The overall fits are consistent with $p_g \propto r^{-1.5}$ and $|b| \propto r^{-1}$ expected for accretion disks, while the shallow density profile could be connected with the stronger wind (relative to the jet) compared to thicker MAD simulations.

4 SUMMARY AND CONCLUSIONS

We have performed fully 3D GRMHD simulations of radiatively efficient thin accretion disks seeking to maximize the magnetically-induced deviations from NT thin disk theory. We first demonstrated that even in thin disks, after a time $108,000r_g/c$ and out to $r \sim 17r_g$, magnetic flux readily advects inward and builds-up to a MAD level (for which accumulation results in magnetic forces pushing out balancing against gas forces pushing in). This occurs despite possible outward magnetic diffusion through the disk.

Our simulation that is MAD out to $r \sim 35r_g$ after $70,000r_g/c$ has a radiative efficiency of $\eta_r \approx 15\%$. This is $\approx 80\%$ higher than the standard NT thin disk value of $\eta_{\text{NT}} \approx 8\%$ and is as if the disk were a standard NT thin disk but with $a/M \approx 0.9$. BH X-ray binaries have $L/L_{\text{Edd}} \sim 0.1$ in the high-soft state (Kulkarni et al. 2011), for which the NT model gives $H/R \lesssim 0.02$ near the BH. Prior non-MAD simulations suggest deviations scale with H/R (Penna et al. 2010), so typical thin MAD deviations might be $\sim 20\%$. Such a magnitude of deviations could slightly impact BH spin measurements, such as in Noble et al. (2011) who found 6% deviations lead to a BH with $a/M = 0$ giving a spectrum like NT but with $a/M \approx 0.3$. Zhu et al. (2012) found that emission from near the ISCO is mostly high-energy, but more physics (e.g., dissipation-radiation energy balance, optical depth effects, BH photon capture) is required for BH spin fitting (Kulkarni et al. 2011). We plan to obtain spectra via post-processing (Zhu et al. 2015). Also, clumpy rest-mass distribution in thin MAD flows may help to explain spectra from AGN (Dexter & Agol 2011) and BH X-ray binaries (Dexter & Quataert 2012).

It is not a new idea that X-ray binaries in the low-hard (LH) state supply enough magnetic flux to the BH to enable BZ-type powering of an observable jet by being geometrically thick, and that the jet quenches when the disk collapses to become thin in the high-soft state. For instance, plunging material inside the ISCO may enhance the flux on the BH in the low-hard state only, even in sub-MAD disks (Reynolds et al. 2006). However, these ideas generally propose transition mechanisms in which the jet is either powered or not, depending on disk state. Our model does not require a special mechanism for the LH state.

Radiatively inefficient flows have $H/R \approx 0.4$ (Narayan et al. 2012). Our fitting formula Eq. (13) suggests that jet power in the MAD state can drop by $\gtrsim (0.4/0.02)^2 \sim 400$ (or drop by $\gtrsim (0.4/0.01)^2 \sim 1600$ for 4U 1957+11 if at $L/L_{\text{Edd}} \approx 0.06$) when undergoing hard-to-soft state transitions. This implies that the observed jet quenching in BH X-ray binaries (Russell et al. 2011) can occur despite the presence of a large-scale MAD-level magnetic field in both disk states. Such hard-to-soft transitions may also be applicable to tidal disruption events at late times (Tchekhovskoy et al. 2014). The MAD state could be necessary to explain powerful jet systems (Zamaninasab et al. 2014), while the thermodynamically determined disk thickness may also play an important role in setting just how much magnetic flux a MAD has. Even thinner

disks than studied here would be implied to have $\Upsilon \propto H/R$ and so could have much weaker magnetic flux and much weaker jets rather than being independent of the disk state.

ACKNOWLEDGMENTS

We thank Ramesh Narayan, Jack Steiner, Roman Gold, Peter Polko, Alexander Tchekhovskoy, and Eliot Quataert for discussions. We acknowledge NASA/NSF/TCAN (NNX14AB46G), NSF/XSEDE/TACC/Stampede (TG-PHY120005), NASA/Pleiades (SMD-14-5451), and UMD Deepthought2.

REFERENCES

- Abramowicz M. A., Chen X., Kato S., Lasota J.-P., Regev O., 1995, *ApJ*, 438, L37
- Balbus S. A., Hawley J. F., 1991, *ApJ*, 376, 214
- Balbus S. A., Hawley J. F., 1998a, *Rev. Mod. Phys.*, 70, 1
- Balbus S. A., Hawley J. F., 1998b, *Reviews of Modern Physics*, 70, 1
- Beckwith K., Hawley J. F., Krolik J. H., 2006, *ArXiv/0605295*
- Beckwith K., Hawley J. F., Krolik J. H., 2009, *ArXiv e-prints*
- Blandford R. D., Payne D. G., 1982, *MNRAS*, 199, 883
- Blandford R. D., Znajek R. L., 1977, *MNRAS*, 179, 433
- De Villiers J.-P., Hawley J. F., 2003, *ApJ*, 589, 458
- De Villiers J.-P., Hawley J. F., Krolik J. H., Hirose S., 2005, *ApJ*, 620, 878
- Dexter J., Agol E., 2011, *ApJ*, 727, L24
- Dexter J., McKinney J. C., Markoff S., Tchekhovskoy A., 2014, *MNRAS*, 440, 2185
- Dexter J., Quataert E., 2012, *MNRAS*, 426, L71
- Fragile P. C., Blaes O. M., Anninos P., Salmonson J. D., 2007, *ApJ*, 668, 417
- Gammie C. F., 1999, *ApJ*, 522, L57
- Gammie C. F., McKinney J. C., Tóth G., 2003, *ApJ*, 589, 444
- Hawley J. F., Guan X., Krolik J. H., 2011, *ApJ*, 738, 84
- Hawley J. F., Richers S. A., Guan X., Krolik J. H., 2013, *ApJ*, 772, 102
- Igumenshchev I. V., 2008, *ApJ*, 677, 317
- Igumenshchev I. V., 2009, *ApJ*, 702, L72
- Igumenshchev I. V., Narayan R., Abramowicz M. A., 2003, *ApJ*, 592, 1042
- Komissarov S. S., McKinney J. C., 2007, *MNRAS*, 377, L49
- Krolik J. H., 1999, *ApJ*, 515, L73
- Kulkarni A. K., Penna R. F., Shcherbakov R. V., et al., 2011, *MNRAS*, 414, 1183
- McClintock J. E., et al., 2011, *Classical and Quantum Gravity*, 28, 114009
- McClintock J. E., Narayan R., Steiner J. F., 2014, *Space Sci. Rev.*, 183, 295
- McKinney J. C., 2005, *ApJ*, 630, L5
- McKinney J. C., 2006, *MNRAS*, 368, 1561
- McKinney J. C., Blandford R. D., 2009, *MNRAS*, 394, L126
- McKinney J. C., Dai L., Avara M., 2015, *ArXiv/1508.02433*
- McKinney J. C., Gammie C. F., 2004, *ApJ*, 611, 977
- McKinney J. C., Narayan R., 2007, *MNRAS*, 375, 513
- McKinney J. C., Tchekhovskoy A., Blandford R. D., 2012, *MNRAS*, 423, 3083
- McKinney J. C., Tchekhovskoy A., Blandford R. D., 2013, *Science*, 339, 49
- McKinney J. C., Tchekhovskoy A., Sadowski A., Narayan R., 2014, *MNRAS*, 441, 3177
- Meier D. L., 2001, *ApJ*, 548, L9
- Narayan R., Igumenshchev I. V., Abramowicz M. A., 2003, *PASJ*, 55, L69
- Narayan R., Sądowski A., Penna R. F., Kulkarni A. K., 2012, *MNRAS*, 426, 3241
- Narayan R., Yi I., 1995, *ApJ*, 452, 710
- Noble S. C., Krolik J. H., Hawley J. F., 2009, *ApJ*, 692, 411
- Noble S. C., Krolik J. H., Hawley J. F., 2010, *ApJ*, 711, 959
- Noble S. C., Krolik J. H., Schnittman J. D., Hawley J. F., 2011, *ApJ*, 743, 115
- Novikov I. D., Thorne K. S., 1973, In *Black Holes-Les Astres Occlus*, ed. C. De Witt & B. S. De Witt, New York: Gordon & Breach
- Penna R. F., McKinney J. C., Narayan R., Tchekhovskoy A., Shafee R., McClintock J. E., 2010, *MNRAS*, 408, 752
- Penna R. F., Sądowski A., McKinney J. C., 2012, *MNRAS*, 420, 684
- Polko P., McKinney J. C., 2015, *ArXiv e-prints*
- Reynolds C. S., et al., 2006, *ApJ*, 651, 1023
- Rothstein D. M., Lovelace R. V. E., 2008, *ApJ*, 677, 1221
- Russell D. M., Miller-Jones J. C. A., Maccarone T. J., et al., 2011, *ApJ*, 739, L19
- Shafee R., McKinney J. C., Narayan R., Tchekhovskoy A., Gammie C. F., McClintock J. E., 2008, *ApJ*, 687, L25
- Shapiro S. L., 2005, *ApJ*, 620, 59
- Shiokawa H., Dolence J. C., Gammie C. F., Noble S. C., 2012, *ApJ*, 744, 187
- Tchekhovskoy A., McKinney J. C., 2012, *MNRAS*, 423, L55
- Tchekhovskoy A., McKinney J. C., Narayan R., 2012, *Journal of Physics Conference Series*, 372, 1, 012040
- Tchekhovskoy A., Metzger B. D., Giannios D., Kelley L. Z., 2014, *MNRAS*, 437, 2744
- Tchekhovskoy A., Narayan R., McKinney J. C., 2011, *MNRAS*, 418, L79
- Zamaninasab M., Clausen-Brown E., Savolainen T., Tchekhovskoy A., 2014, *Nature*, 510, 126
- Zhu Y., Davis S. W., Narayan R., Kulkarni A. K., Penna R. F., McClintock J. E., 2012, *MNRAS*, 424, 2504
- Zhu Y., Narayan R., Sądowski A., Psaltis D., 2015, *MNRAS*, 451, 1661